Chain motion in amorphous regions of polyethylene: interpretation of deuteron n.m.r. line shapes

K. Rosenke†, H. Sillescu and H. W. Spiess
Institut für Physikalische Chemie der Universität Mainz, Sonderforschungsbereich Chemie und Physik der Makromoleküle, Mainz/Darmstadt, D-6500 Mainz, W. Germany
(Received 28 December 1979)

The motion of $(-CD_2-)_N$ chains with fixed ends has been simulated in a diamond lattice for variable chain lengths and end-to-end distances. The deuteron n.m.r. line shape was calculated for various motional constraints. Motional narrowing of experimental n.m.r. spectra between room temperature and the melting point of deuterated polyethylene can be understood by a simple model chain. The model assumes rapid motion of short subchains between entanglements which move slowly but allow for further line narrowing at higher temperature.

INTRODUCTION

Molecular motion in solid polyethylene (PE) has been investigated extensively by application of n.m.r. methods, in particular wide line[1,2] and spin lattice relaxation[3] studies of ^{1}H–n.m.r. (most of the earlier literature cited in these papers), and, more recently, of ^{13}C–[4,5] and ^{2}D–n.m.r.[6,7].

The analysis of ^{1}H–n.m.r. in terms of particular motional models is difficult since it entails the problem of dipolar interaction between many protons. Furthermore, there is no unambiguous procedure for separating the contributions from protons in the crystalline and amorphous regions, respectively. Proton spin lattice relaxation times T_1 are strongly influenced by spin diffusion effects[8]. Thus, the T_1 values reflect end group rotation at low temperatures, whereas, at high temperatures, the contributions from protons in crystalline regions (α-process) become considerable[3,8]. Recently, ^{13}C–n.m.r. has been studied in PE by Mandelkern and collaborators[4,5]. Here, the relaxation times T_1 and the line shapes* are determined purely by intramolecular contributions, and can be treated readily by model calculations discussed in the present paper.

The observable entities of ^{2}D–n.m.r. are governed by nuclear quadrupole coupling of the deuteron with the electric field gradient that originates from the C–D σ-bond, all other couplings contributing only a few percent in deuterated PE[6]. Relaxation and motional narrowing are related directly to motions of the C–D vector. The line shape of rigid deuterons is the 'Pake spectrum'[9]. Thus, the crystalline contribution can be subtracted from the total line shape of partially crystalline PE. This is possible even at temperatures where the α-process occurs in the crystalline regions, since 180° jumps have no influence on ^{2}D–n.m.r.[9]. Former ^{2}D–n.m.r. investigations of solids have been hampered by low signal-to-noise ratios. Recent advances have overcome this difficulty. By using cryomagnets, the ^{2}D Larmor frequency can be increased to the values of former ^{1}H frequencies, e.g. 55 MHz at 8.5 T. An even more drastic noise reduction is possible through the Fourier transform solid echo technique[7] which is well suited for deuterated polyethylene (PED) since the short spin lattice relaxation time T_1 allows for repetition times of the order of seconds. An observable solid echo in the amorphous regions of PED proves the existence of motional constraints with a life time longer than the pulse distance of the solid echo sequence. Further information on chain dynamics is available from spin lattice relaxation times T_1 which can be studied separately for the amorphous and the crystalline regions in PED, and from the response to the Jeener 3 pulse sequence[10], sensible to slow molecular motions[11].

Simulation of chain motion in a diamond lattice[12,13] is compared favourably with ^{2}D–n.m.r. line shapes since the possible directions of the C–D vectors coincide with the 4 tetrahedral axes of the lattice. Thus, *any* chain motion in the lattice is seen from the viewpoint of ^{2}D–n.m.r. as a special mechanism for producing tetrahedral jumps of the C–D vectors. Since the 'rapid motion limit' (proven by the existence of solid echos) applies to the amorphous regions of PED, the ^{2}D line shape is determined uniquely if the probabilities w_i (i = 1, 2, 3, 4) of finding the C–D vector in one of its 4 possible orientations are known for each deutron of the model chain. Within the limit of a completely flexible chain, all w_i are equal to 1/4, resulting in complete narrowing of the spectrum into a δ-function line at the ^{2}D Larmor frequency. At the other extreme, a fully extended chain is fixed to its all-*trans* conformation where one of the w_i equals unity for each deuteron, and the line shape becomes the 'Pake spectrum' of the rigid limit. In a chain with fixed ends, the probabilities w_i are different because of motional constraints that are most severe for short chains, and for longer but relatively extended chains.

The purpose of our line shape calculations is to obtain some estimate of the length of flexible chain segments bet-

† Present address: Firma Grundig, D-8510 Fürth, W. Germany

* Additional broadening by field inhomogenity and probe geometry has been avoided in present investigations (private communication with Professor Mandelkern)

0032-3861/80/070757-07$02.00

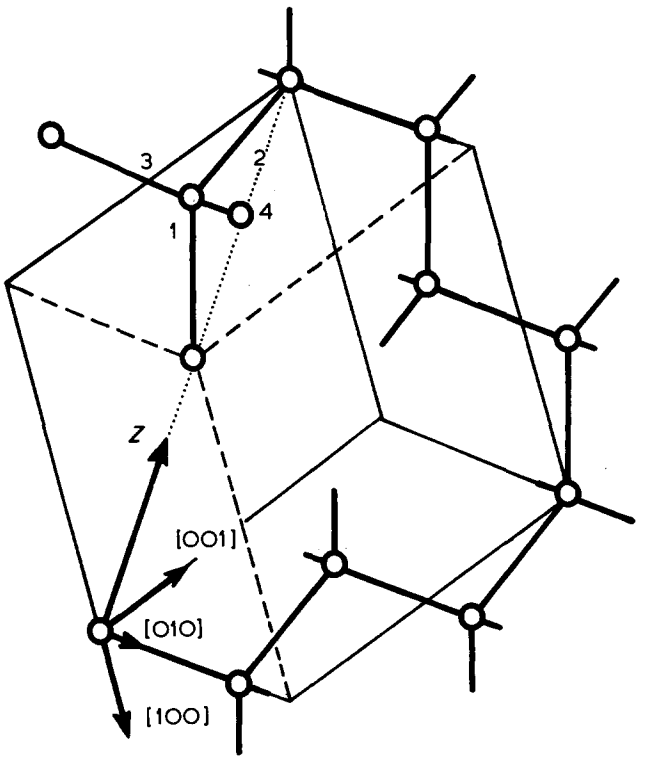

Figure 1 Carbon chain in the diamond lattice, $N = 11$, $h/h_0 = 0.2$. Tetrahedral directions: 1 = [11$\bar{1}$], 2 = [$\bar{1}$11], 3 = [$\bar{1}\bar{1}$1], 4 = [1$\bar{1}$1]. Coordinate system *x, y, z*: the axes *y* = [010] and *z* = [$\bar{1}$01] (. . . . .) are shown

ween points that are 'fixed' with respect to the time scale of the solid echo sequence (about 0.1 ms). The fixed C-atoms exist at the surface of the PE crystals and as 'entanglements' within the amorphous regions. Line width decreases drastically on heating PED in a region between room temperature and the melting point: from this experimental observation, we have to conclude that an increasing number of 'fixed' C-atoms become mobile with respect to our time scale. These findings have motivated our design of the model described in the following section. Although this model may appear highly artificial at first sight, it will be shown that it contains the essential features of chain motion in the amorphous regions of PE.

MODEL TREATMENT OF CHAIN MOTION

Chains between fixed ends

A model chain constrained to the diamond lattice is characterized by the number N of C-atoms, and the end-to-end vector **h**. In most of our calculations, we assume that **h** is parallel to one of the 6 (positive) directions that are possible for all-*trans* chains in the diamond lattice, namely, [101], [$\bar{1}$01], [110], [1$\bar{1}$0], [011], and [0$\bar{1}$1]. In particular, [101] and [$\bar{1}$01] are chosen as *x*- and *z*-axes, respectively, of a lattice-fixed right-handed rectangular system *x, y, z* (*Figure 1*). We define the relative end-to-end distance by h/h_0 where h_0 is the distance for an all-*trans* chain. There are 4 possible C–D directions for each deuteron of the chain labelled by numbers 1–4 given by the tetrahedral axes [11$\bar{1}$], [$\bar{1}$11], [$\bar{1}\bar{1}$1], and [1$\bar{1}$1], respectively; the corresponding negative directions are irrelevant in our context.

For given values of N and h/h_0, the most flexible chain is obtained by neglecting excluded volume effects, and assuming that all accessible conformations are equally probable. Using these assumptions, Schmedding and Zachmann[14] have calculated the orientational probabilities of methylene H–H directions in order to interpret ^{1}H–n.m.r. in PEH. We have adopted their methods for calculating the corresponding probabilities w_i (i = 1, 2, 3, 4) for the C–D directions in PED. Thus, all possible conformations for given N and h are constructed, and for each deuteron α the fraction of conformations having the α C–D bond in direction i is determined:

$$w_i = w_i(N, h, \alpha)$$

As mentioned in the Introduction, and explained more fully in the following section, the ^{2}D–n.m.r. line shape is determined uniquely by the set of probabilities w_i.

The number of possible conformations becomes prohibitively large for $N > 13$. Thus, we have used a Monte Carlo method in order to obtain a random selection of conformations for one longer chain, $N = 21$. Starting from the 1st (fixed) C-atom on the *z*-axis, a particular conformation is obtained by determining consecutively the directions of the 20 C–C bonds. The direction is determined at random for each step. If a 'backstep' occurs that implies a zero C–C–C bond angle, the conformation is omitted. Furthermore, only those conformations where the 21st C–atom is at one of the 6 possible all-*trans* chain axes through the 1st atom are maintained. The ensemble of chains constructed by this procedure has a Gaussian distribution of end-to-end distances from which subensembles for particular h/h_0 values are obtained.

Line shape calculations have been performed also for modified model chains that are subject to the following assumptions:

(a) excluded volume: each position of the lattice is occupied by only one C-atom.

(b) intramolecular interaction: according to the rotational isomeric state model[15], the conformations are weighted by the Boltzmann factor $\exp(-E_g/RT)$ for each *gauche* bond where $E_g \approx 2$ kJ mol^{-1} and T = 300K. Furthermore, the 'pentane effect' is accounted for by a weight factor with energy values between 7 and 10 kJ mol^{-1} for each g^+g^- combination in the conformation considered;

(c) variable bond angles: the bond angles in a real PE chain are somewhat different from the tetrahedral angle of 109.47°, and the 3 rotation angles around a C–C bond (0°, ± 120°) may fluctuate by as much as ±10° due to the shape of the rotational potential[16]. We have simulated deviations from the tetrahedral angle as follows. In an ensemble of $N = 21$ chains with equal h/h_0 we change the bond- and rotation-angles at one end by small random values whereby the long rest chains leave the diamond lattice. The same is done for each chain with the 2nd bond keeping the 1st bond fixed, and so on. Finally, all bond angles are changed, and the bond directions at the 'other end' of a chain may deviate considerably from one of the tetrahedral axes of the initial diamond lattice. Furthermore, the h/h_0 values will now have a distribution around the value of the initial ensemble;

(d) 3-bond motion and crankshaft rotation: conformational changes due to 3-bond motions have been studied extensively by Monnerie and collaborators[12]. In *Figure 2a*, the bonds 1, 2, 3 are transferred by a 3-bond motion into 1′, 2′, 3′ whereby the kink defect at bond 1 moves to 3′. In our simulations, we use $N = 21$ chains with a fixed h/h_0 value. In each step, a random generator determines the posi-

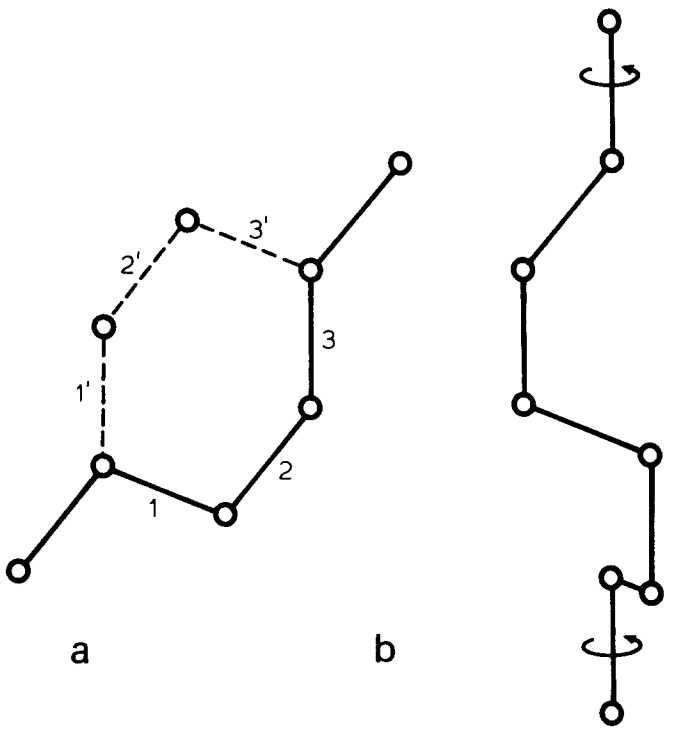

Figure 2 (a) 3-bond motion and (b) crankshaft rotation in the diamond lattice

tion at the chain where a 3-bond motion should occur. If the motion is possible, it leads to a new conformation. If it is not possible, the old conformation is counted twice. In this manner, 10 000 steps are performed on each chain, generating an ensemble of conformations with appropriate weights. The ^{2}D–n.m.r. spectrum is determined for each chain from conformations generated by this procedure. Only a relatively small number of conformations is accessible through 3-bond motions from a given initial conformation. Thus, the 3-bond motion alone is a poor mechanism for causing motional narrowing of n.m.r. spectra. Below, we shall discuss further the n.m.r. line shapes generated through 3-bond motions.

The mechanism of crankshaft rotation permits only 3 equally probable directions for each C–D bond of the 8 C-atoms shown in *Figure 2b*. The resulting 'motional narrowing' is also discussed below.

Entangled chains

In order to simulate chains which have additional motional constraints, let us consider an ensemble of 100 chains with $N = 51$ C-atoms. Each chain is partitioned into 21 subchains by selecting $n = 20$ C-atoms at random, each becoming the 'fixed end' of 2 subchains. For each subchain, the end-to-end distance h is chosen at random from the relatively small number of possible h values. The direction of the **h** vector of each subchain is chosen at random from the 12 directions that are possible for all-*trans* chains in the diamond lattice (see above). By this procedure, we obtain an ensemble of 100 approximately Gaussian chains with $N = 51$, and an average ratio of $\langle h/h_0 \rangle = 0.19$. Due to the 20 fixed C-atoms (in addition to the fixed end C-atoms), the chains are rather rigid since only a small number of conformations is accessible. The resulting rather broad n.m.r. spectrum (see below) describes the situation of bulk PE at room temperature. In order to obtain a more flexible chain, one of the 'fixed' C-atoms is chosen at random in each chain, and the corresponding constraint is removed. Thus, the average lengths of the subchains become longer, and more conformations become accessible for the $N = 51$ chains. By successive removal of more constraints on the 'fixed' C-atoms, one attains the complete flexibility available for a chain with fixed ends. The corresponding motionally-narrowed line shapes correspond to experimental n.m.r. spectra close to the melting point of PE.

N.M.R. SPECTRA

Line shapes

In high magnetic fields, the ^{2}D–n.m.r. spectrum is governed by the first order nuclear quadrupole splitting of the ^{2}D Larmor frequency. The quadrupole Hamiltonian can be written as[9]:

$$\mathscr{H}_Q = \tfrac{1}{4}e^2Qq\, \underset{\sim}{I}\cdot\underset{\sim}{R}\cdot\underset{\sim}{I} \qquad (1)$$

where e^2Qq is the quadrupole coupling constant, $\underset{\sim}{I} = (I_\xi, I_\eta, I_\zeta)$ is the spin vector of the deuteron in some cartesian coordinate system ξ, η, ζ. For a C–D bond fixed in space, $\underset{\sim}{R}$ is a tensor given by:

$$\underset{\sim}{R}_{PAS} = \begin{pmatrix} -1 & 0 & 0 \\ 0 & -1 & 0 \\ 0 & 0 & 2 \end{pmatrix} \qquad (2)$$

in its principal axes system (PAS) where the C–D bond is the unique axis. Above (*Figure 1*), we have defined a coordinate system x, y, z that is fixed to the diamond lattice. In this system

$$\underset{\sim}{R}(1) = \begin{pmatrix} -1 & 0 & 0 \\ 0 & 0 & -\sqrt{2} \\ 0 & -\sqrt{2} & 1 \end{pmatrix};\ \underset{\sim}{R}(2) = \begin{pmatrix} -1 & 0 & 0 \\ 0 & 0 & \sqrt{2} \\ 0 & \sqrt{2} & 1 \end{pmatrix}$$

$$\underset{\sim}{R}(3) = \begin{pmatrix} 1 & \sqrt{2} & 0 \\ \sqrt{2} & 0 & 0 \\ 0 & 0 & -1 \end{pmatrix};\ \underset{\sim}{R}(4) = \begin{pmatrix} 1 & -\sqrt{2} & 0 \\ -\sqrt{2} & 0 & 0 \\ 0 & 0 & -1 \end{pmatrix} \qquad (3)$$

for the 4 orientations given in *Figure 1*. (Due to the symmetry of $\underset{\sim}{R}$ the sign of the orientations is irrelevant).

Any conformational transition of the model chain gives rise to exchange of the C–D bond between the 4 possible orientations. For the rapid motion limit, the n.m.r. line shape is obtained from the time-averaged Hamiltonian:

$$\overline{\mathscr{H}}_Q = \tfrac{1}{4}e^2Qq\, \underset{\sim}{I}\cdot\underset{\sim}{\bar{R}}\cdot\underset{\sim}{I} \qquad (4)$$

where $\underset{\sim}{R}$ of equation (1) is replaced by the average $\underset{\sim}{\bar{R}}$ given in the x, y, z-system by:

$$\underset{\sim}{\bar{R}} = \sum_{i=1}^{4} w_i \underset{\sim}{R}(i) \qquad (5)$$

$$= \begin{pmatrix} -w_1 - w_2 + w_3 + w_4 & \sqrt{2}(w_3 - w_4) & 0 \\ \sqrt{2}(w_3 - w_4) & 0 & \sqrt{2}(w_2 - w_1) \\ 0 & \sqrt{2}(w_2 - w_1) & w_1 + w_2 - w_3 - w_4 \end{pmatrix}$$

The weight factors w_i were defined in the Introduction; they are proportional to the average times spent by the C–D bond in the 4 possible tetrahedral directions (see *Figure 1*). Diagonalization of the traceless tensor $\underset{\sim}{\bar{R}}$ yields the directions of the principal axes X, Y, Z, the principal component $\bar{R}_{ZZ}$, and the asymmetry parameter $\bar{\eta} = (\bar{R}_{YY} - \bar{R}_{XX})/\bar{R}_{ZZ}$. The 2 n.m.r. frequencies that correspond to the $1 \leftrightarrow 0$ and $0 \leftrightarrow -1$ transitions of the ^{2}D spin $I = 1$ depend upon $\bar{R}_{ZZ}$, $\bar{\eta}$, and the orientation of the external magnetic field with respect to the system X, Y, Z. In order to simulate the line shape of a polycrystalline sample (or glass), one has to compute a superposition of the doublets obtained above with weight factors that correspond to the orientational distribution of the X, Y, Z-systems fixed to the individual microcrystals. This can readily be performed using the method discussed by Hentschel *et al.*[17]. In the present paper, we consider only isotropic orientational distributions where the normalized 'powder' line shape has been given by Bloembergen and Rowland[18] as:

$$f(\omega) = f_+(\omega) + f_-(\omega) \tag{6}$$

$$f_+(\omega) = \pi^{-1}[(\omega_3 - \omega_2)(\omega - \omega_1)]^{-1/2} K \left\{ \arcsin \left[\frac{(\omega_3 - \omega)(\omega_2 - \omega_1)}{(\omega_3 - \omega_2)(\omega - \omega_1)} \right]^{1/2} \right\} \tag{7}$$

for $\omega_3 > \omega \geqslant \omega_2$;

$$f_+(\omega) = \pi^{-1}[(\omega_3 - \omega)(\omega_2 - \omega_1)]^{-1/2} K \left\{ \arcsin \left[\frac{(\omega_3 - \omega_2)(\omega - \omega_1)}{(\omega_3 - \omega)(\omega_2 - \omega_1)} \right]^{1/2} \right\} \tag{8}$$

for $\omega_2 \geqslant \omega > \omega_1$;

$$f_-(\omega) = f_+(-\omega) \tag{9}$$

$$K(\arcsin x) = F(x, \pi/2) \tag{10}$$

is the complete elliptic integral of the 1st kind[19]. ω_1, ω_2, and ω_3 are proportional to the principal components of the averaged tensor $\underset{\sim}{\bar{R}}$. For each particular deuteron of a model chain, the n.m.r. line shape has the form given by $f(\omega) = f_+(\omega) + f_+(-\omega)$ [see equations (6–10)]. A typical example of $f_+(\omega)$ is shown in *Figure 3b*. For an axially symmetric $\underset{\sim}{\bar{R}}$-tensor ($\eta = 0$), the singularities at ω_1 and ω_2 coincide, and $f(\omega)$ becomes the Pake spectrum shown in *Figure 3a*. This line shape is obtained for the mechanism of *crankshaft rotation* (*Figure 2*). Here $\omega_i = 1/3$ for 3 orientations, and 0 for the 4th orientation along the rotation axis. Thus $\underset{\sim}{\bar{R}}$ defined in equation (5) is just 1/3 of one of the R-tensors given in equation (3) for rigid C–D bonds, and the line shapes become identical except for the reduced width by a factor of 1/3 that is due to 'motional narrowing' through crankshaft rotation.

In the other limiting case, $\eta = 1$, the ω_2-singularity becomes the centre of a symmetrical spectrum, $f(\omega) = 2f_+(\omega) = 2f_+(-\omega)$, shown in *Figure 3c*. This shape is found for the 3-bond motion (see *Figure 2*) where each C–D bond jumps between two orientations, the other two being inaccessible. Thus, $\omega_1 = \omega_2 = 1/2$, $\omega_3 = \omega_4 = 0$, and averaged tensor $\underset{\sim}{\bar{R}}$, given in equation (5), has only two non-vanishing components, $\bar{R}_{XX} = -1$ and $\bar{R}_{ZZ} = 1$, hence $\eta = 1$.

If the line shapes for all individual C–D bonds in a chain are superimposed, one obtains the calculated ^{2}D–n.m.r. spectrum for this particular model. The broadest of the superimposed shapes are due to the deuterons at the fixed end C-atoms, since they are the least flexible. This is opposite to free chains in melts and solutions where the end groups are the most flexible.

The small magnetic dipolar coupling between neighbouring deuterons can be accounted for by convoluting the spectra discussed above with a Gaussian, where the width is estimated from the 2nd moment of the ^{1}H–n.m.r. spectrum[6]. Some further broadening is justified if small deviations from the tetrahedral orientations of the diamond lattice are taken into consideration. In accordance with experiment, the width of the Gaussian is kept below 1% of the total width of the spectrum, and thus leads only to some smoothing of the singularities.

Dynamical aspects

The line shapes discussed above are independent of any motional correlation times, since we have assumed the rapid motion limit where all possible conformational transitions are rapid with respect to the n.m.r. time scale. The following discussion aims to give a quantitative measure of this time scale.

In the rigid limit, the ^{2}D quadrupole coupling constant in PED is $e^2Qq/h = 164$ kHz[20]. The total width of the Pake spectrum (*Figure 3a*) is $3/2e^2Qq/h$. A measure of the line shape that is more relevant to motional narrowing is the 2nd moment:

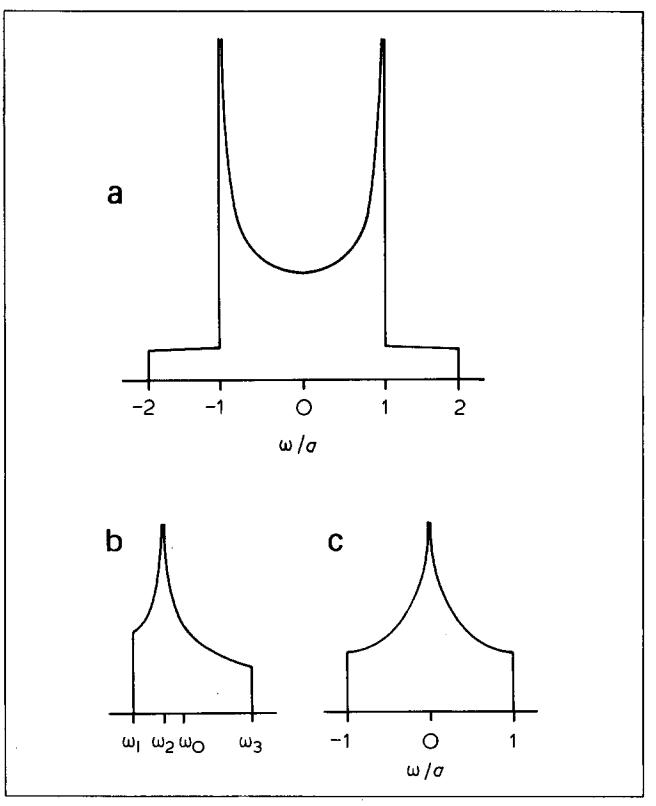

Figure 3 (a) Pake spectrum of rigid deuterons in PED. $a/2\pi = 3/8e^2Qq/h = 61.5$ kHz; (b) example of the line shape $f_+(\omega)$ defined in equations (7) and (8). ω_0 is the Larmor frequency; (c) line shape for $\eta = 1$; deuterons of C–D bonds performing two site jumps in the diamond lattice

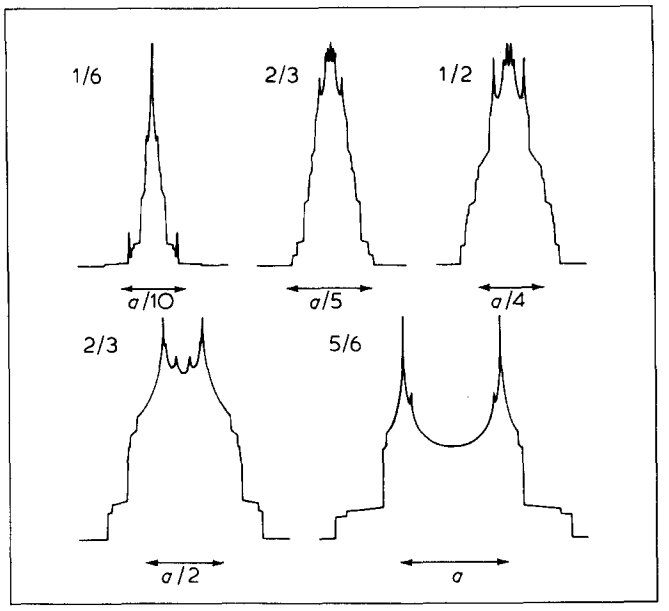

Figure 4 Line shape for $N = 13$ chains. Numbers denote the values of h/h_0, bars the value of a defined in the legend of Figure 3

$$M_2 = \int_0^\infty (\omega - \omega_0)^2 f(\omega)\mathrm{d}\omega \Big/ \int_0^\infty f(\omega)\mathrm{d}\omega \qquad (11)$$

where $f(\omega)$ is defined in equation (6) and ω_0 is the Larmor frequency. For spectra obtained from the time averaged Hamiltonian $\bar{\mathscr{H}}_Q$ [see equation (4)], the 2nd moment is:

$$\bar{M}_2 = \frac{9}{80}\pi^2(e^2Qq/h)^2\bar{R}_{ZZ}^2(1 - \bar{\eta}^2/3) \qquad (12)$$

where the bar upon $\bar{M}_2$ indicates the time average. (In the rigid limit, $\bar{R}_{ZZ} = R_{ZZ} = 2$ and $\bar{\eta} = \eta = 0$).

In order to understand the increasing motional narrowing as the temperature is raised, let us now consider a hierarchy of motional processes with correlation times:

$$\tau_c^{(1)} \ll \tau_c^{(2)} \ll \ldots \ll \tau_c^{(\max)} \qquad (13)$$

If we denote by $\bar{M}_2^{(1)}$ the time average of M_2 due to the process with $\tau_c^{(1)}$, the line shape corresponds to the rapid motion limit if†:

$$(M_2 - \bar{M}_2^{(1)})\tau_c^{(1)2} \ll 1 \qquad (14)$$

As an example for a process with small $\tau_c^{(1)}$ we may consider two site jumps of the C–D bond yielding the $\bar{\eta} = 1$ spectrum with $\bar{R}_{ZZ} = 1$ (see *Figure 3c*). Here, equation (12) yields $M_2 = 1.2 \times 10^{11}\ \mathrm{s}^{-2}$ and $\bar{M}_2^{(1)} = 4.0 \times 10^{10}\ \mathrm{s}^{-2}$; thus, the inequality (14) requires $\tau_c^{(1)} \ll 3.5 \times 10^{-6}$ s.

A slower process with $\tau_c^{(2)}$ does not influence the line shape calculated from $\bar{\mathscr{H}}_Q^{(1)}$ provided:

$$(\bar{M}_2^{(1)} - \bar{M}_2^{(2)})\tau_c^{(2)\,2} \gg 1 \qquad (15)$$

† For isotropic reorientation, $\bar{M}_2 = 0$ and $1/T_2 = M_2\tau_c$ is the half-width of the narrow Lorentzian line obtained in the rapid motion limit where $\tau_c/T_2 = M_2\tau_c^2 \ll 1$. A possible generalization of this condition for anisotropic motion is given by the inequality (14)

where the average $\bar{M}_2^{(2)}$ includes both processes with $\tau_c^{(1)}$ and $\tau_c^{(2)}$. An estimate of $\tau_c^{(2)}$ is given by the smallest 'homogeneous' half-width $1/T_2'$ that would be found in a single crystal. The solid echo technique provides a method for estimating T_2' in a polycrystalline sample, since the Fourier transform of the solid echo is only identical with the absorption spectrum if the time τ between the two 90° pulses of the solid echo sequence is smaller than T_2' [7,21]. By investigating solid echo *FT*-spectra as a function of τ one can determine the order of magnitude of $T_2' \approx \tau_c^{(2)}$ experimentally, and check whether the inequality (15) holds. If (15) breaks down, further narrowing occurs, and one may attain the rapid motion limit:

$$(\bar{M}_2^{(1)} - \bar{M}_2^{(2)})\tau_c^{(2)2} \ll 1$$

By increasing the temperature of the sample, all motions become more rapid, and inequalities:

$$(\bar{M}_2^{(k-1)} - \bar{M}_2^{(k)})\tau_c^{(k)2} \ll 1; h = 2, 3, 4, \ldots \qquad (16)$$

become valid consecutively for all processes of the hierarchy with the correlation times $\tau_c^{(1)}, \tau_c^{(2)}, \ldots, \tau_c^{(\max)}$. It should be noted that $\tau_c^{(k)}$ can be larger than $\tau_c^{(1)}$ by almost two orders of magnitude since the higher averages $\bar{M}_2^{(k-1)}$ become rather small for the narrowed lines as can be inferred from *Table 1*. Finally, we should mention that $\tau_c^{(\max)}$ can be determined separately from the response of the Jeener 3 pulse sequence[10,11] provided $\tau_c^{(\max)}$ is smaller than the spin lattice relaxation time T_1.

RESULTS AND DISCUSSION

Chains between fixed ends

The motional constraints given by the fixed end C-atoms in the diamond lattice are most severe for very short chains. No motion is possible for $N = 3$, and only two site jumps of the C–D bond are possible for $N = 4$ that give rise to the $\eta = 1$ spectrum shown in *Figure 3c*. This spectrum is then superimposed upon the Pake spectrum (*Figure 3a*) for C–D bonds with the same orientation in all possible chain conformations. For longer chains, the number of accessible conformations increases rapidly, leading to considerable motional narrowing if h/h_0 is sufficiently small. In *Figure 4*, the $N = 13$ spectra are shown for all h/h_0 values (see *Figure 3a* for $h/h_0 = 1$) that are possible if both end C-atoms are fixed to the z-axis defined in *Figure 1*. We have omitted the broader line shape contributions of the deuterons at the fixed ends since they become less important for larger N-values whereas the line shapes shown in *Figure 4* are typical for all $N \geqslant 11$ in that the half-widths (and the 2nd moments, see *Table 1*) have approximately the same dependence upon the parameter

Table 1 Comparison of the 2nd moment ratios $\bar{M}_2/M_2$ for ^{1}H– and ^{2}D–n.m.r. line shapes, $N = 13$. $M_2(^2\mathrm{D}) = 1.19 \times 10^{11}\ \mathrm{s}^{-2}$, $M_2(^1\mathrm{H}) = 1.74 \times 10^{10}\ \mathrm{s}^{-2}$

h/h_0	$\bar{M}_2/M_2(^1\mathrm{H})$	$\bar{M}_2/M_2$ (^{2}D)
1/6	0.0005	0.0003
1/3	0.0040	0.0018
1/2	0.0220	0.0097
2/3	0.1132	0.0624
5/6	0.4182	0.3271
1	1.0000	1.0000

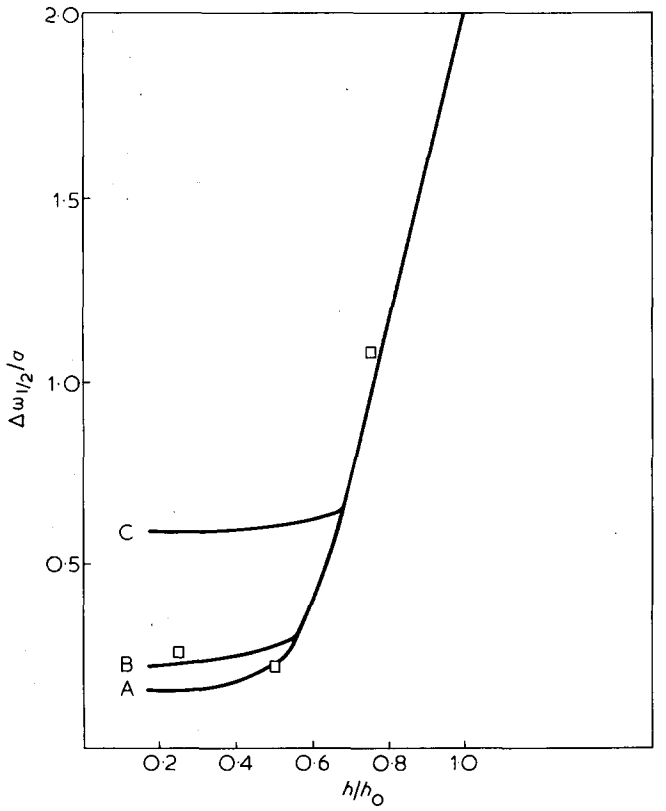

Figure 5 Half-width at half-height $\Delta\omega_{1/2}$ of the ^{2}D–n.m.r. spectra calculated for chains with fixed ends, and $N \geqslant 11$; A, no excluded volume (squares are for $N = 9$ chains); B, excluded volume of C-atoms; C, intramolecular interaction (see text)

h/h_0 (see *Figure 5*). This has been confirmed by our Monte Carlo calculations for $N = 21$ where some further narrowing is only obtained for $h/h_0 < 0.2$.

The second moment of the ^{2}D– and ^{1}H–n.m.r. line shapes in PED and PEH, respectively, have been calculated for $N = 13$ chains as a function of h/h_0. We conclude from the results given in *Table 1* that the tetrahedral jumps of C–D bonds provide a more effective line narrowing mechanism than the corresponding jumps of methylene group H–H vectors between the six orientations possible in the diamond lattice.

The *excluded volume* effect where two carbons cannot occupy the same site in the diamond lattice is shown in *Figure 5* for $N = 13$ chains. There is no excluded volume for $h/h_0 \geqslant 0.5$ since these rather extended chains cannot fold back upon themselves. However, some broadening occurs for $h/h_0 < 0.5$. For $N = 21$, the excluded volume effect on the line shape is negligible since there is always a sufficient number of conformations available for motional narrowing.

The influence of *intramolecular interaction* (conformational energies) is shown also in *Figure 5* for $N = 13$ chains. The additional broadening originates almost completely from exclusion of g^+g^- combinations by the weight factor $\exp(-E_{g^+g^-}/RT)$ where $E_{g^+g^-} \geqslant 7$ kJ mol^{-1}. This may be regarded as another 'excluded volume effect' since it prohibits conformations where two deuterons would occupy the same site in the diamond lattice.

Variable bond angles have been simulated as described above. Starting from an ensemble of $N = 21$ chains with equal h/h_0, this procedure results in a distribution of h/h_0-values similar to those discussed by Cook and Moon[16]. Thus, the average $\langle h/h_0 \rangle$ is smaller than the initial h/h_0 for more extended chains, and it is increased compared with the initial h/h_0 if the latter is small. The influence of bond angle variation on the *shape* of the n.m.r. spectrum is small. Therefore, the spectrum calculated for some $\langle h/h_0 \rangle$ value corresponds to the spectrum calculated in the undistorted diamond lattice for an *effective* $h/h_0 = \langle h/h_0 \rangle$.

The effect of *3-bond motions* on the n.m.r. spectrum is shown in *Figure 6* for $N = 21$ and $h/h_0 = 0.20$. We have also calculated the spectrum for $h/h_0 = 0.60$, and have found it almost identical with *Figure 6*. This triangular line shape is typical for jumps of C–D bonds between only two sites though the spectrum is narrower than the $\eta = 1$ spectrum shown in *Figure 3c* for *3-bond* motion in an $N = 4$ chain. Thus, kink diffusion along the chain seems to be restricted to rather short chain segments irrespective of the h/h_0-value. Since the n.m.r. line widths found experimentally[6,21] in the amorphous regions of PE close to the melting point are narrower by a factor of 50 than the width of *Figure 6*, there must be other motions that cause the further line narrowing. At first sight, this seems to be at variance with publications of Gény and Monnerie[12] where only *3-bond* motions are assumed in PE. However, 3-bond motion is a very rapid process with typical correlation times around 10^{-11} s. Other motions discussed above in terms of a hierarchy of correlation times $\tau_c^{(2)}, \tau_c^{(3)}, \ldots$ may be effective line narrowing processes although they are highly improbable in comparison with 3-bond motion, and have correlation times longer by perhaps four orders of magnitude.

Entangled chains

The ^{2}D–n.m.r. spectra calculated for our model of entangled chains are shown in *Figure 7*. It is clear that the most constrained chains ($n = 20$) almost have the rigid limit 'Pake spectrum' (*Figure 3a*) since most of the C–D bonds are fixed. For $n = 16$, the fraction of very short chains is still predominant. This results in a line shape that is a superposition of the rigid limit spectrum and the $\eta = 1$ spectrum (*Figure 3c*) for 2 site jumps of the C–D bonds. With further decreasing n, one obtains superpositions of spectra for subchains with increasing N. For subchains having $N > 13$, we have assumed the corresponding $N = 13$ spectra since the line widths and shapes are approximately the same for all spectra with equal h/h_0 if $N \geqslant 11$ (see *Figure 5*). Furthermore, we have neglected the effects of excluded volume and the conformational energies discussed above. Nevertheless, motional narrowing of the calculated spectra with decreasing n reflects real motional narrowing in PED between room temperature and the melting point[6,21]. In particular, the line

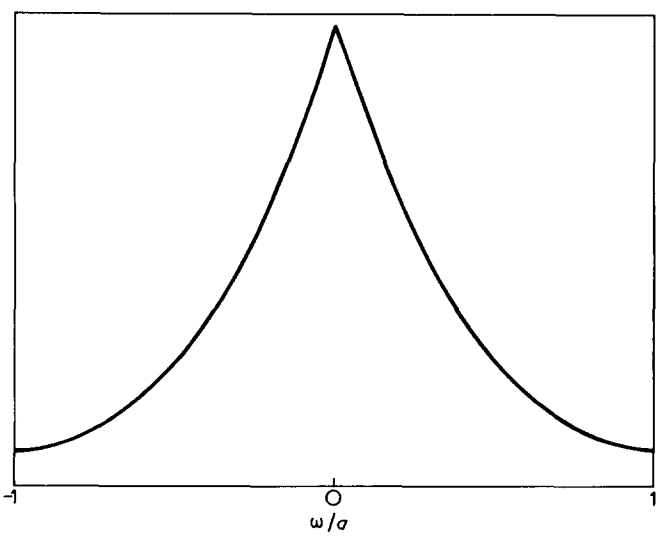

Figure 6 Line shape for 3-bond motion in $N = 21$ chains, $h/h_0 = 0.2$

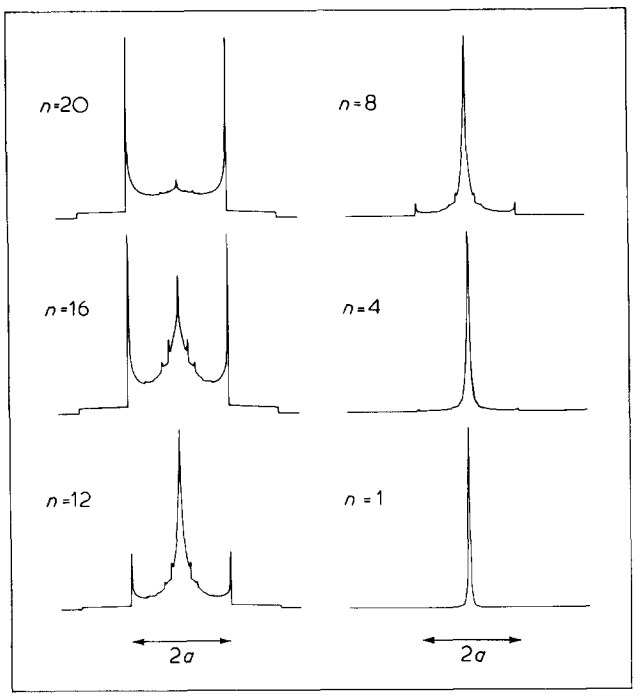

Figure 7 Line shapes for entangled $N = 51$ chains. n is the number of fixed entanglement points

widths for small n have the same order of magnitude as the line width in PED above 100°C. The most significant difference is found in the relative intensity of the mobile fraction of the n.m.r. spectra. In real PED, this intensity depends little upon temperature and corresponds essentially to all deuterons in the amorphous regions[6]. On the other hand, the calculated line shapes have a substantial 'rigid' portion down to small n values where the central part of the spectrum becomes narrow. This must be considered as an artefact of the diamond lattice where the probability that a C–D bond has the same orientation through all accessible conformations is exaggerated.

Dynamics of chain motion has been considered above in terms of a hierarchy of motional processes with correlation times $\tau_c^{(1)}, \tau_c^{(2)}, \ldots, \tau_c^{(k)}, \ldots, \tau_c^{(\max)}$ subject to inequality (13). We have seen that even moderate line narrowing (found in PED at room temperature) requires a rather short correlation time $\tau_c^{(1)} < 10^{-6}$ s in order to fulfil inequality (14). This is in agreement with measurements of the spin lattice relaxation time T_1 of ^{2}D in PED yielding correlation times not longer than 10^{-7} s.

On the other hand, $\tau_c^{(2)}$ must be at least of the order of 10^{-4} s since the solid echo Fourier Transform spectra remain undistorted for pulse distances $\tau \leqslant 10^{-4}$ s between the two 90° pulses of the solid echo pulse sequence[21]. Thus, inequality (15) can be fulfilled; this supports our conception of rapid motion of short chain pieces between points that are 'fixed' as we have seen, for $\geqslant 10^{-4}$ s. At higher temperatures, motion of the entanglements becomes faster, and further line narrowing is observed. However, there may remain 'slow' entanglements with correlation times $\tau_c^{(k)} \geqslant$ above 100°C since the *preaveraged* spectra can be averaged further by additional processes with correlation times $\tau_c^{(k)}$ that are much larger than $\tau_c^{(1)}$ [see discussion below inequality (16)]. Since the Jeener 3-pulse sequence produces spin alignment for a time distance up to 50 ms at temperatures close to the melting point of PED, the largest correlation time $\tau_c^{(\max)}$ must be at least of this order[11]. This is understood by noting that the chains are fixed at the crystal surfaces in the partially crystalline PED since we find no spin alignment above the melting point.

The description of chain motion by essentially two time scales agrees with other models. In the reptation model[22,23], one assumes curvilinear diffusion of the chain within a 'tube' formed by the surrounding chains. This wormlike 'reptation' is caused by Brownian motion of chain length defects that will also give rise to transitions of the C–D bonds resulting in some narrowing of the ^{2}D-n.m.r. spectrum similar to the narrowing by two site jumps (*Figure 3c*) or 3-bond motion (*Figure 6*). The motion of a flexible tube[23] will also reorient the C–D bonds of the embodied chain, and lead to further narrowing of the spectrum. Since the tube constraints correspond to the chain entanglements considered above, the physical reason for line narrowing is the same in both models. Reptation within a *rigid* tube[22] cannot explain the narrow lines found experimentally in PED above 100°C, since sufficient reorientation can then be achieved only by *translational* diffusion of the C–D bonds along the chain over a distance of the order of the correlation length of the tube (~1 nm in polymer melts[24,25]). Since the chain ends are fixed at the crystal surface boundaries of the amorphous regions in solid PE, it is difficult to imagine the motion of a particular CD_2 group along this distance.

REFERENCES

1 McBrierty, V. J. and McDonald, I. R. *Polymer* 1975, **16**, 125
2 Bergmann, K. *J. Polym. Sci. (Polym. Phys. Edn)* 1978, **16**, 1611
3 Voigt, G. and Kimmich, R. *Progr. Colloid Polym. Sci.* 1979, **66**, 273
4 Komoroski, R. A., Maxfield, J., Sakaguchi, F. and Mandelkern, L. *Macromolecules* 1977, **10**, 550
5 Axelson, D. E. and Mandelkern, L. in 'Carbon-13 NMR and Solving Problems in Macromolecular Chemistry', *ACS Monograph Series*, in press
6 Hentschel, D., Sillescu, H. and Spiess, H. W. *Makromol. Chem.* 1979, **180**, 241
7 Hentschel, R. and Spiess, H. W. *J. Magn. Resonance* 1979, **35**, 157
8 Heaberlen, U. *Kolloid Z. Z. Polym.* 1968, **225**, 15
9 Abragam, A. 'The Principles of Nuclear Magnetism', Oxford University Press, Oxford, 1961
10 Jeener, J. and Broekaert, P. *Phys. Rev.* 1967, **157**, 232
11 Spiess, H. W. *J. Chem. Phys.* in press
12 Gény, F. and Monnerie, L. *J. Polym. Sci. (Polym. Phys. Edn)* 1979, **17**, 131, 147 and references cited therein
13 Rosenke, K. and Zachmann, H. G. *Progr. Colloid Polym. Sci.* 1978, **64**, 245 and references cited therein
14 Schmedding, P. and Zachmann, H. G. *Kolloid Z. Z. Polym.* 1972, **250**, 1105
15 Flory, P. J. 'Statistical Mechanics of Chain Molecules', Interscience, New York, 1969
16 Cook, R. and Moon M. *Macromolecules* 1978, **11**, 1054
17 Hentschel, R., Schlitter, J., Sillescu, H. and Spiess, H. W. *J. Chem. Phys.* 1978, **68**, 1
18 Bloembergen, N. and Rowland, T. J. *Acta Metall.* 1953, **1**, 731
19 Abramowitz, M. and Stegun, I. A. (Eds.), 'Handbook of Mathematical Functions', New York, 1970
20 Hentschel, D., Silloscu, H., Spiess, H. W., Voelkel, R. and Willenberg, B. *Magn. Reson. Relat. Phenom., 19th Proc. Congr. Ampère* 1976, p 381
21 Hentschel, D., Spiess, H. W. and Sillescu, H. to be published
22 De Gennes, P. G. *J. Chem. Phys.* 1971, **55**, 572
23 De Gennes, P. G. *Macromolecules* 1976, **9**, 587, 594
24 Kimmich, R. *Polymer* 1975, **16**, 851
25 Koch, H. and Kimmich, R., communication presented at IUPAC International Symposium on Macromolecules, Mainz, 1979